IOPscience iopscience.iop.org

Home Search Collections Journals About Contact us My IOPscience

Enhancement of plasma wakefield generation and self-compression of femtosecond laser pulses by ionization gradients

This content has been downloaded from IOPscience. Please scroll down to see the full text.

2014 Plasma Phys. Control. Fusion 56 084010

(http://iopscience.iop.org/0741-3335/56/8/084010)

View the table of contents for this issue, or go to the journal homepage for more

Download details:

IP Address: 141.213.19.93
This content was downloaded on 09/12/2014 at 20:34

Please note that terms and conditions apply.

IOP Publishing
Plasma Physics and Controlled Fusion
Plasma Phys. Control. Fusion **56** (2014) 084010 (7pp)
doi:10.1088/0741-3335/56/8/084010

Enhancement of plasma wakefield generation and self-compression of femtosecond laser pulses by ionization gradients

Z-H He, J A Nees, B Hou, K Krushelnick and A G R Thomas

Center for Ultrafast Optical Science, University of Michigan, Ann Arbor, MI 48109, USA

E-mail: zhhe@umich.edu

Received 6 December 2013, revised 3 April 2014
Accepted for publication 2 May 2014
Published 22 July 2014

Abstract
As lasers become progressively higher in power, optical damage thresholds will become a limiting factor. Using the non-linear optics of plasma may be a way to circumvent these limits. In this paper, we report on simulations showing an enhancement to plasma wakefield self-compression of femtosecond laser pulses due to an ionization gradient at the leading edge of the pulse. By operating in a regime where wakefield generation is driven by moderately relativistic ($\sim 10^{18}$ W cm^{-2}) laser pulses and proper choice of gas species, the ionization front of the pulse can lead to a frequency shift that enhances the ponderomotive force and therefore both the wakefield generation and subsequent pulse compression.

Keywords: laser, plasma, accelerators, compression, femtosecond

(Some figures may appear in colour only in the online journal)

1. Introduction

Generation of intense few-cycle pulses is of great interest in high-field science in areas such as laser driven particle acceleration [1] and attosecond pulses from high-order harmonic generation [2]. Kerr nonlinearity and/or ionization-induced phase modulation have been utilized as sources of spectral broadening in plasma filaments [3], gas-filled waveguides [4], and bulk media [5] in previous experimental and theoretical work. Compensation for dispersion of a light pulse in a medium is possible by using additional dispersive optical elements such as chirped mirrors, by self-compression schemes in a filament [3] or multi-dimensional spatio-temporal reshaping mechanism in a plasma medium [4, 6]. A relativistically intense pulse driving a plasma wave can also lead to self-compression [7–14]. It is, however, an important and challenging problem to achieve homogenous temporal pulse compression with a focusable spatial profile and high energy throughput efficiency. In addition, demonstration of a high degree of pulse stability is of crucial importance.

For a slowly varying (compared with the laser frequency) laser envelope and density perturbation, the refractive index in a plasma is given by $\eta = \sqrt{1 - \omega_{pr}^2(\boldsymbol{r})/\omega_0^2}$, where $\omega_{pr}(\boldsymbol{r}) = \sqrt{e^2 n_e/(\langle\gamma\rangle m_e \epsilon_0)}$ is the local plasma frequency for electron density n_e, with the averaged Lorentz factor $\langle\gamma\rangle$ arising as a consequence of the quiver energy of electrons in the laser focus. In a relativistically intense laser focus, $I \gg 10^{17}$ W cm^{-2}, both the variation in $\langle\gamma\rangle$ and the density modulation of the plasma wave generated by the ponderomotive expulsion of electrons give rise to gradients in refractive index. As a consequence, the laser frequency is shifted on the gradients in such a way that self-compression occurs via group velocity dispersion (GVD). This type of compression can be effective, but previous results have demonstrated low transmission [11, 12]. For lower pulse intensity, $I < 10^{17}$ W cm^{-2}, ionization-induced nonlinearities can also be used for spectral broadening and pulse compression [4, 6, 15]. However, since ionization also results in a transverse refractive index variation, compensation for the defocusing of the pulse must be done by using an external guiding structure [4].

In this paper, we study the effect of direct laser ionization in the self-compression of relativistically intense laser pulses in a laser generated plasma wakefield using particle-in-cell (PIC)

© 2014 IOP Publishing Ltd Printed in the UK

simulations. Operating in a moderately relativistic regime with $a_0 \sim 1$, where $a_0 = eA/m_ec$ is the normalized vector potential (corresponding to an intensity of approximately 2×10^{18} W cm^{-2} for 800 nm light), we observed more than over-two-fold pulse compression of a 35 fs pulse produced by a tightly focused Ti : Sapphire based chirped pulse amplification (CPA) laser system at pulse energy level as low as multi-millijoule. A thin plasma (∼100 μm scalelength) was used to match the short Rayleigh distance associated with a relatively tight focusing geometry. We will show that an enhancement of the wakefield generation occurs due to the ionization gradient nonlinearity at the pulse front, which therefore also enhances pulse compression. This enhancement was also observed using a much higher pulse energy with a larger focal spot as the ionization front behaves similarly with the same gas. Hence, we demonstrate that this method can be easily scaled to work with a wide range of laser energies.

2. Numerical experiments

Simulations were performed using the two-dimensional (2D) PIC code OSIRIS 2.0 [16]—a fully explicit relativistic electromagnetic PIC code that includes a suite of ionization physics models. The PIC approach contains the full range of electromagnetic and collisionless plasma physics, yet the nonlinear response of bound electrons in atoms and molecules such as the Kerr effect is not included in the code. Although the nonlinear refractive index is important at lower intensities, as the plasma ionizes, the ratio of third order susceptibilities for the ion relative to the neutral atom, $\chi_i^{(3)}/\chi_0^{(3)}$, scales as the ratio of ionization potentials cubed, $(U_0/U_i)^3$ [17], where U_0 is the ionization potential of the neutral atom and U_i is that of an ion with charge state i. Therefore, it rapidly becomes negligible compared with the plasma refractive index as the plasma ionizes. The ionization rate typically increases very rapidly with laser intensity. It should be pointed out that for the laser intensity in our simulations, the laser pulse begins to ionize the gas a few hundred μm before the laser focus. Therefore, given the scalelength of the gas profile, the self-phase modulation contributed by Kerr nonlinearity may be considered negligible. This validates the use of PIC for the computational experiments under the parameters considered here.

Simulations were carried out in a moving window of dimensions 64 μm × 230 μm on a Cartesian grid with step sizes $\Delta x = \lambda/12$ (the propagation direction) and $\Delta y = \lambda/5$ (the transverse direction). The transverse dimension is chosen to be sufficient to contain the large diffraction angle of a tightly focused laser beam. Ionization physics can be optionally included using the ADK tunnel ionization model [18]. For each ionization level, particles with a charge-to-mass ratio equivalent to that of an electron were used, with 4×4 particles-per-cell. The maximum available ionization level is 2 and 8 for helium and argon respectively. Alternatively, the electrons can be initiated in the simulations with neutralizing immobile ions to model the case of a pre-formed plasma with no ionization effects. The electron or neutral density profile has a truncated Gaussian profile with a FWHM width of 150 μm to simulate a realistic gas jet. When using different gas species, the peak density is chosen such that the plasma has the same electron density when the maximum ionization level is reached.

We first simulated a 10 mJ pulse, a full-width-at-half-maximum pulse duration of 37 fs propagating in a gas or plasma with a peak plasma density, n_e, ranging from 0 to $0.07n_c$ using tunnel-ionizable argon gas, where $n_c = 1.74 \times 10^{21}$ cm^{-3} is the plasma critical density for 800 nm light The laser is focused in the ascending part of the Gaussian density profile.

The transverse pulse profile and the magnitude of the peak intensity of the output laser pulse is shown in figure 1 with the spatial-temporal intensity distribution depicted in three-dimensional surface plots. At higher densities ($n_e > 0.05n_c$), the laser pulse begins to suffer modulational instability and breaks up into sub-pulses as seen in figure 1(*d*)–(*e*).

Simulations were performed using the same laser conditions and electron densities with a pre-formed plasma as well as a neutral helium gas. Along with the case of argon, the results are shown in figure 2 for the output pulse width as a function of the peak plasma density. First we define the pulse width τ using the peak intensity of the output pulse I_{out} normalized to the intensity of the same input pulse propagating in vacuum, I_{vac}, as $\tau = \tau_0 I_{\mathrm{vac}}/I_{\mathrm{out}}$, where $\tau_0 = 37$ fs is the initial FWHM pulse duration. Note this definition incorporates transverse effects such as self-focusing, plasma defocusing and filamentation instability. To quantify the complicated sub-pulse structures especially at higher densities, we also plot using a RMS pulse width definition, given by $2.36\sqrt{\langle I^2\rangle - \langle I\rangle^2}$, where $\langle I^n\rangle = \int_{-\infty}^{\infty} t^n I(t)\,\mathrm{d}t / \int_{-\infty}^{\infty} I(t)\,\mathrm{d}t$ is the n-th moment of the temporal intensity profile. A constant scaling factor of 2.36 is used to normalize the result to the FWHM pulse duration of a Gaussian pulse (initial pulse profile). The optimal density for the maximal homogeneous compression occurs at about 0.05 n_c, which yields the highest peak intensity after compression. This can be also seen from figure 1(*c*). Under the same conditions, the use of argon plasma results in a compressed pulse that is 25% shorter than that of pre-ionized or helium plasma, but may be more susceptible to plasma defocusing or beam break-up at higher densities.

We examine the Wigner distribution [19] to visualize the local frequency distribution within the pulse. The results are plotted in figure 3 for the laser pulse at the end of the simulation for the cases of vacuum, pre-ionized plasma, helium and argon. For the same electron density (fully ionized), argon exhibits more spectral broadening, especially a greater red shift compared to the pre-ionized and helium cases. Ionization blueshift [20] at the pulse front is also discernible in figures 3(*c*) and (*d*).

This effect can be utilized at higher pulse energies by simply increasing the spot size to maintain the same ionization gradient at the pulse front for a specific choice of gas. In figure 4, we show the on-axis pulse evolution with ionization (from argon) and without (pre-formed plasma) for both the low energy case and a high energy pulse. A laser pulse of 36 fs duration and 1 J energy passes through a short argon plasma. A slightly shorter plasma with a Gaussian width of 120 μm instead of 150 μm is used to avoid detrimental beam break-up that we observe for the longer propagation distance. This is because the high energy pulse has a longer Raleigh range for

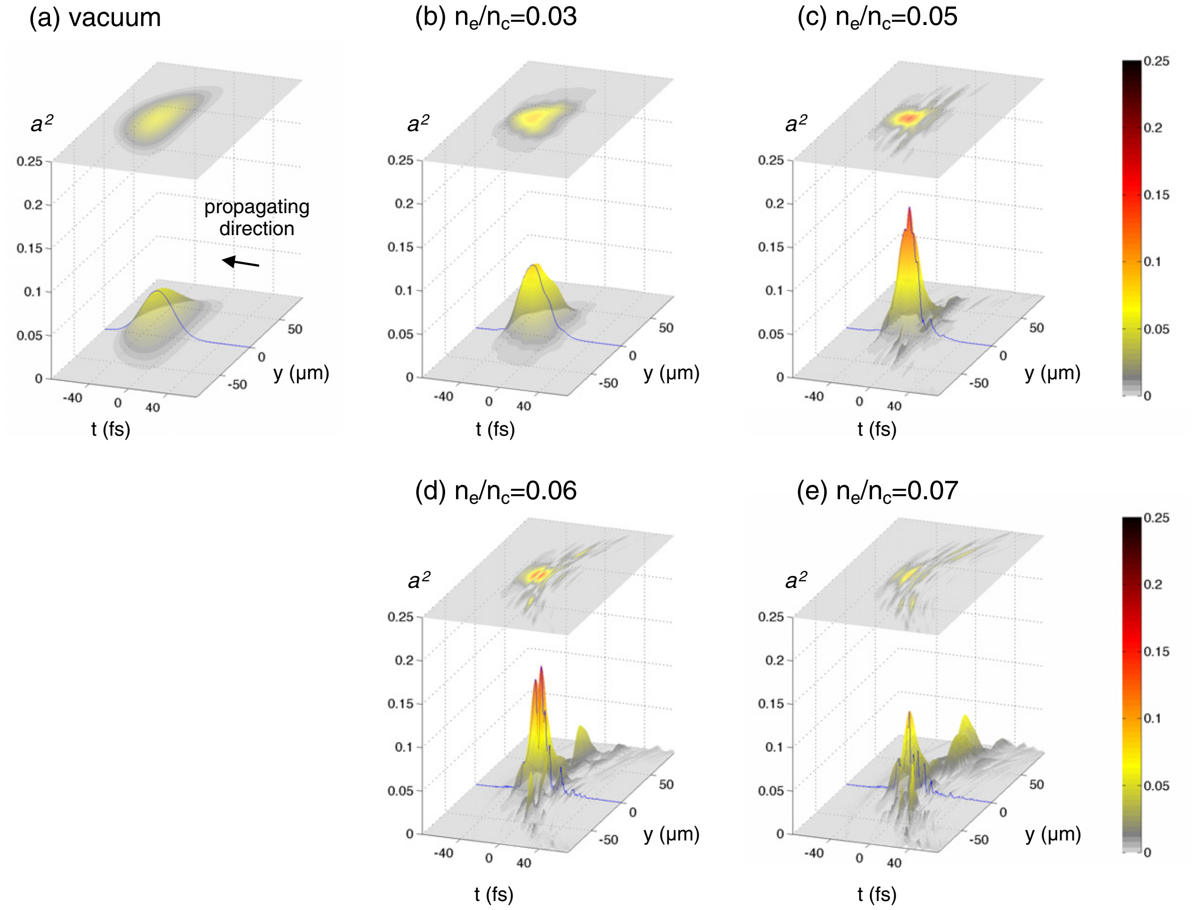

Figure 1. Simulation of a 37 fs (FWHM pulse width), 10 mJ pulse propagating through an argon plasma that has a Gaussian density profile. (*a*)–(*e*) The intensity distributions of the pulse at the end of the simulation with a peak electron density $n_e = 0$(vacuum), $0.03n_c$, $0.05n_c$, $0.06n_c$, $0.07n_c$.

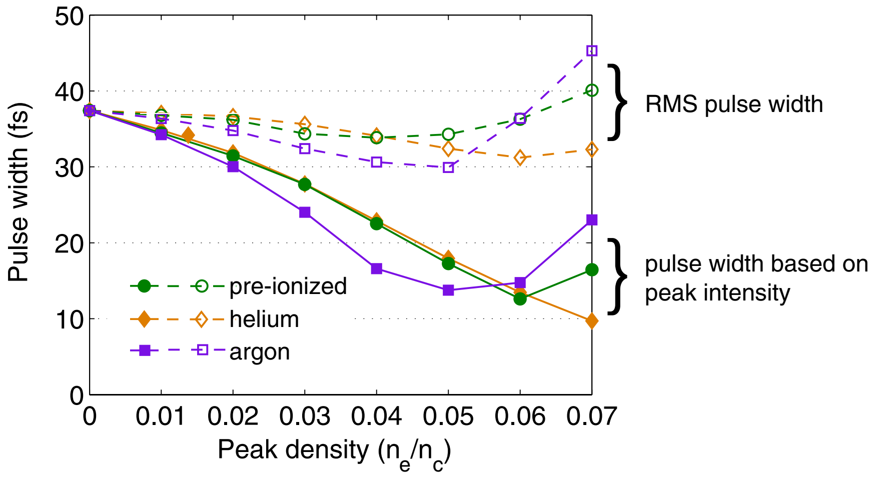

Figure 2. The output pulse duration as a function of electron density for a pre-ionized plasma (circles) and tunnel-ionizable gases of helium (diamonds) or argon (squares). Filled points/solid lines are plotted for the pulse width based on the peak intensity and empty points/dashed lines are for the RMS pulse width.

the same focused intensity and therefore longer for transverse focusing instabilities to develop. A focal diameter (FWHM) of 30 μm is used in order to provide a peak intensity close to that of the low energy case. The high energy pulse becomes similarly self-compressed to 15 fs and 22 fs with argon and pre-formed plasma respectively.

Figure 5 shows the spatial distribution of the high energy compressed pulse. The spatial profile of the pulse retains good transverse homogeneity without filamentation due to the short plasma length. Thus we have demonstrated the energy scalability of this concept by showing that in both the low and high energy pulse cases, the peak power/intensity has been

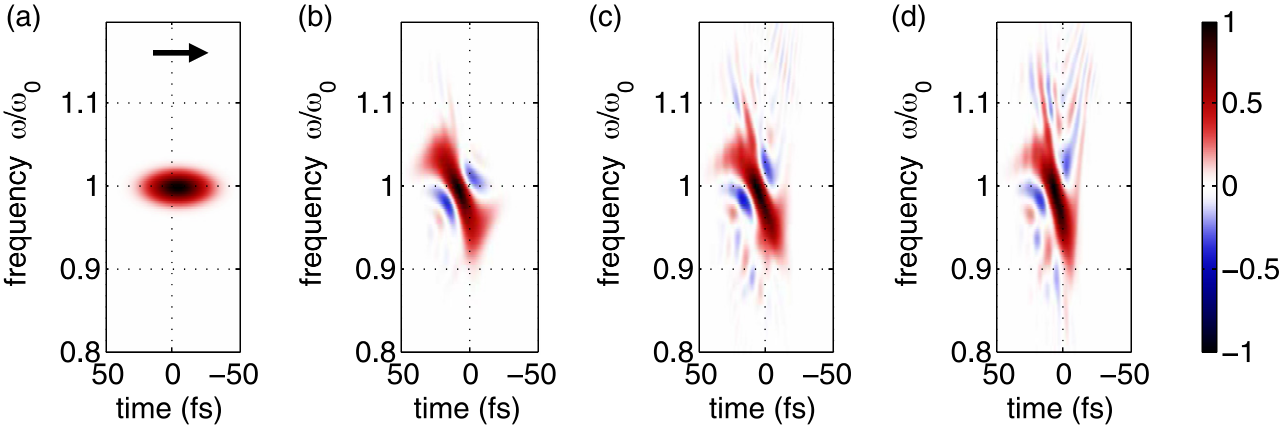

Figure 3. Wigner distributions of the laser pulse at the end of the simulations for: (*a*) propagation in vaccum; (*b*) pre-ionized plasma; (*c*) helium and (*d*) argon. (*b*)–(*d*) have the same electron density profile when ionized (peak $n_e = 0.05n_c$). The arrow indicates the propagation direction.

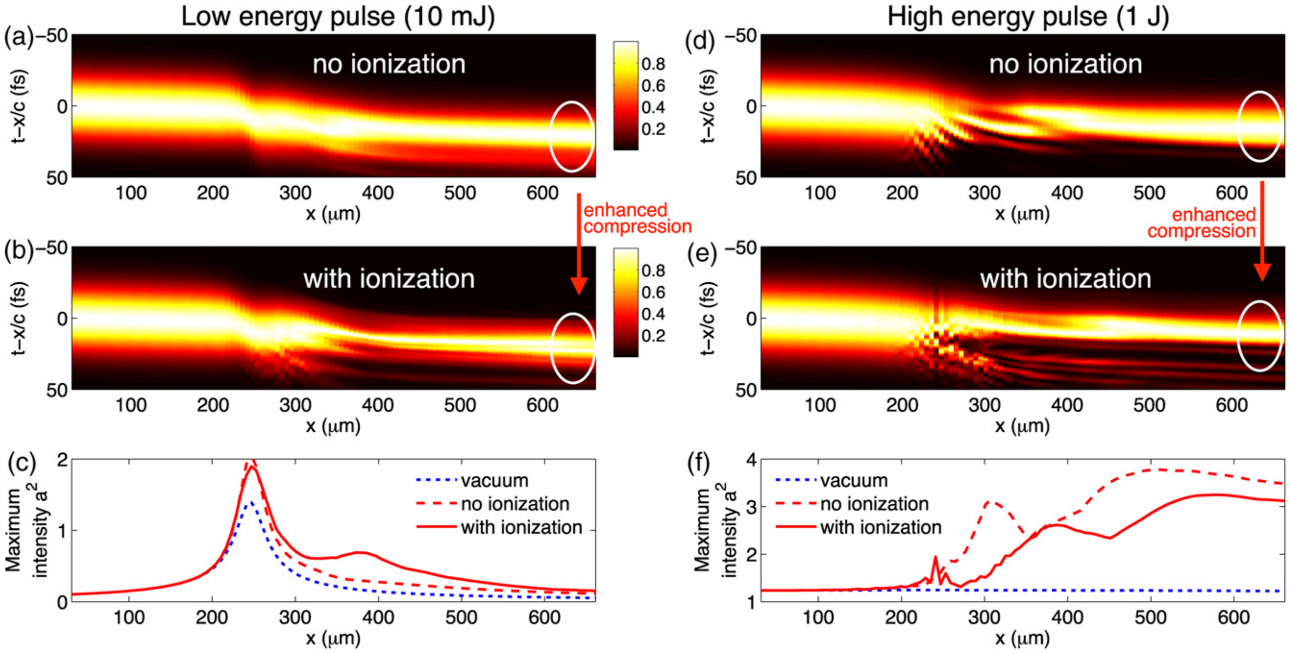

Figure 4. The evolution of the on-axis temporal intensity profile along the propagation direction x in the PIC simulations. The peak intensity has been normalized to 1 at every spatial slice to the compression of the laser pulse. (*a*)–(*c*) are shown for a low energy pulse (10 mJ) focused to a spot size of 2.5 μm and (*d*)–(*f*) for a high energy pulse (1 J) with a larger focal spot size (30 μm). The actual peak intensity value (red solid/dashed lines) is plotted in panel (*c*) and (*f*) for both cases together with the reference vacuum scenario (blue dotted line). Data shown are with a peak electron density $n_e = 0.05n_c$ located at 300 μm.

doubled with a similar compression factor, stemming from the same ionization gradient.

3. Discussion

These simulations suggest that the ionization process plays a significant role in enhancing pulse compression, despite the main mechanism being from a combination of relativistic self-phase modulation and wakefield generation. As it propagates, the leading edge of the pulse generates a strong ionization gradient that causes blue-shifting of the front of the pulse. The resulting group velocity dispersion in the plasma leads to the front edge developing a steep gradient, as the blue shifted portion separates from the main pulse. This portion represents only a small amount of energy at the foot of the pulse. However, an almost discontinuous change in frequency develops, from red shifted to blue shifted with respect to the fundamental frequency, as the pulse crosses from the upward density ramp of the wakefield to the downward ramp of the ionization gradient. As a result, a feedback loop occurs, whereby the steep gradient in E^2/ω^2 enhances the ponderomotive force, thereby generating a larger amplitude wakefield compared to the situation with no ionization effects. This in turn leads to further red shifting of the front of the pulse within the wakefield, thus enhancing the effect.

The plasma waves in the wake of the laser pulse are shown in figure 6 by plotting the on-axis electron density profiles from

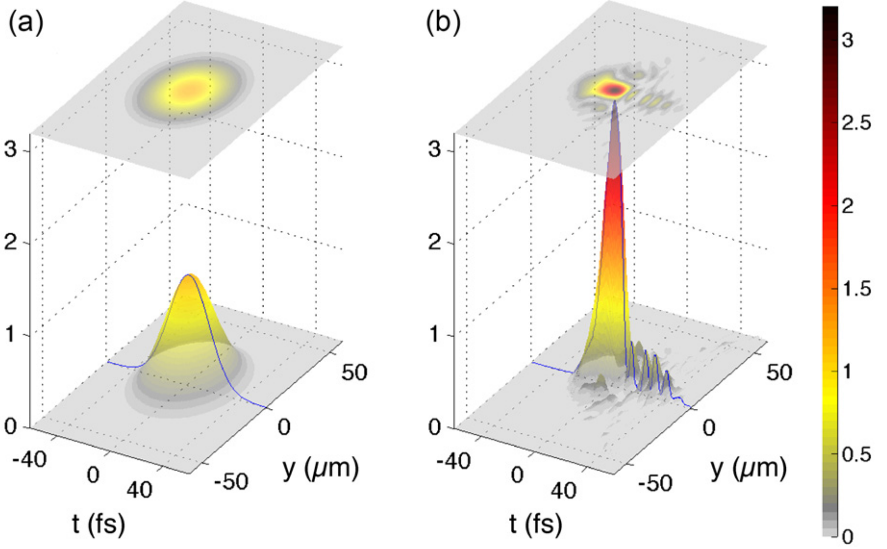

Figure 5. The intensity distribution of a 1 J pulse after propagating in (*a*) vacuum (*b*) argon plasma with a peak electron density $n_e = 0.05n_c$. The FWHM focal size is 30 μm.

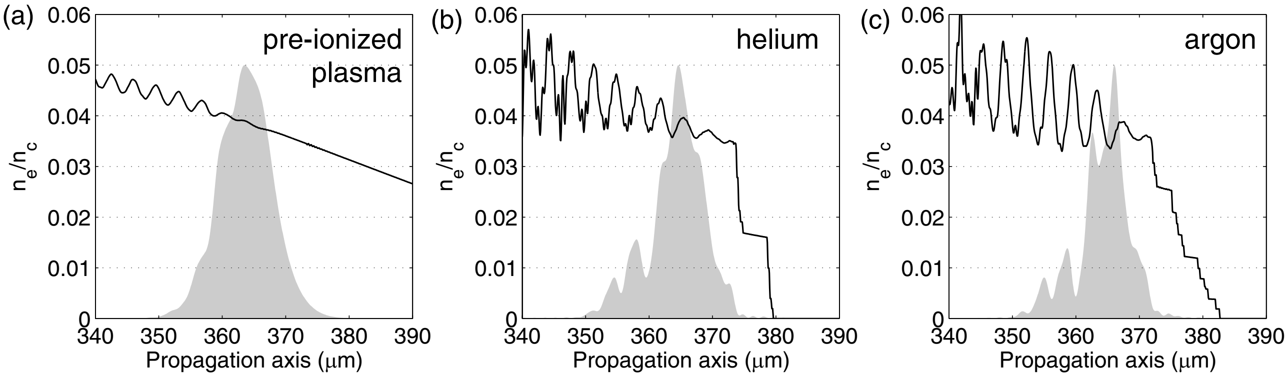

Figure 6. On axis electron density profiles at the propagation distance about 370 μm shown for (*a*) pre-ionized plasma (*b*) helium (*c*) argon. The shaded area represents the pulse intensity profiles normalized to the same pulse height.

our 2D simulations with 10 mJ laser pulse using pre-ionized plasma, helium and argon. Significant wakefield amplitude enhancement can be seen due to the ionization of helium/argon.

The wave equation in the presence of an ionization front can be expressed in terms of the wave frame coordinates $\xi = z - ct$ and $\tau = t$ and is given by [21]

$$\left(2c\frac{\partial}{\partial\xi} - \frac{\partial}{\partial\tau}\right)\frac{\partial}{\partial\tau}E(\xi,\tau) = \omega_p^2(\xi,\tau)E(\xi,\tau), \qquad (1)$$

where $\omega_p^2(\xi,\tau) = e^2n_e(\xi,\tau)/m_e\epsilon_0$ is the local plasma frequency. Using a slowly varying envelope approximation, the solution for the amplitude of the electric field is

$$E(\tau) = E_0\frac{\omega_0}{\omega(\tau)}, \qquad (2)$$

where E_0 is the initial electric field and the time varying frequency is

$$\omega(\tau) = \left(\omega_0 + \frac{1}{\xi}\int_0^\tau \omega_p^2(\xi,\tau')\,\mathrm{d}\tau'\right)^{1/2}. \qquad (3)$$

The vector potential $A(\tau)$ is therefore related to the electric field, equation (2), by

$$A(\tau) = A_0\frac{{\omega_0}^2}{\omega(\tau)^2}. \qquad (4)$$

This situation is in contrast to the situation of a pulse on a density up-ramp due to a wakefield perturbation, in which case the vector potential is given by $A(\tau) = A_0\omega_0/\omega(\tau)$ (i.e. conserving photon number), with a similar expression for $\omega(\tau)$ [21].

The generalized relativistic ponderomotive force is [22]

$$\frac{\mathrm{d}\langle \boldsymbol{p}\rangle}{\mathrm{d}t} = -\frac{e^2}{2m\langle\gamma\rangle}\nabla\langle A^2\rangle, \qquad (5)$$

where the angle brackets denote the time average over a laser period. For the phase dependent frequency shifts a cycle average is more difficult to define, however it can be shown that for a single electron in a plane wave, expressed in terms of the vector potential in the Coulomb gauge, the Lorentz force

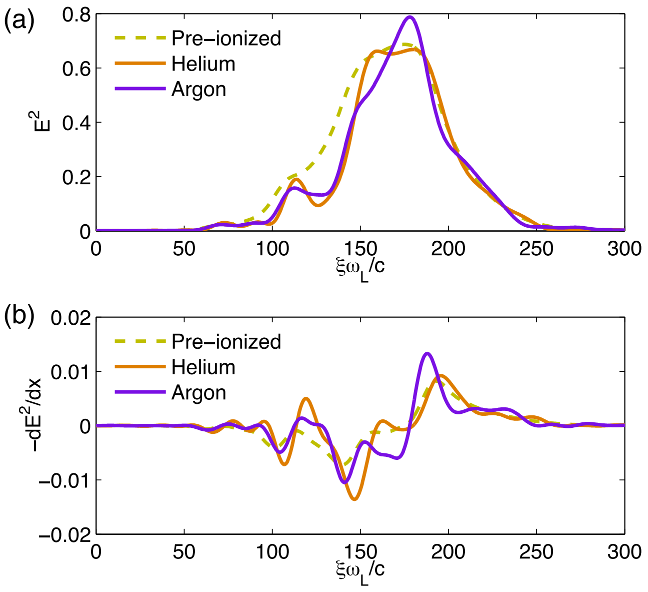

Figure 7. (*a*) The intensity envelope of a 1D laser pulse after propagating through a 300 μm plasma with a density of $n_e = 0.024n_c$. (*b*) The spatial derivative of the intensity envelope showing the ponderomotive force. The pulse is propagating to the right.

can be expressed in the exact form

$$\frac{d\boldsymbol{u}}{d\tau} = -\frac{e^2}{2m\gamma}\hat{\boldsymbol{k}}\frac{\partial}{\partial\xi}\left(A^2\right), \tag{6}$$

where $\boldsymbol{u} = \boldsymbol{p} - e\boldsymbol{A}$ is the canonical momentum, $\hat{\boldsymbol{k}}$ is the direction of wave propagation and no averaging has been performed. Inserting equation (4) into equation (6);

$$\frac{d\boldsymbol{u}}{d\tau} = -\frac{e^2}{2m\gamma}\hat{\boldsymbol{k}}\frac{\partial}{\partial\xi}\left(A_0^2\frac{{\omega_0}^4}{\omega(\tau)^4}\right), \tag{7}$$

This expression indicates that the longitudinal force in the presence of ionization gradients depends inversely on the gradient in $\omega(\tau)^4$ relative to the envelope without frequency shifts, ${A_0}^2$. It is therefore very sensitive to the ionization-induced frequency shift.

We performed one-dimensional (1D) PIC simulations to understand the ionization gradient effect on the ponderomotive force. Since this simple model eliminates multi-dimensional effects as well as any density gradient effect by using a uniform density profile, the 1D pulse has a peak $a_0 = 0.8$ and propagates in a uniform plasma with $n_e = 0.024n_c$. The intensity envelope of the pulse is shown in figure 7(*a*) for the three cases of a pre-ionized plasma, helium and argon. We plot the spatial derivative $-\partial E^2/\partial x$ in figure 7(*b*) using the electric field from the simulation. Although this expression is not precisely the ponderomotive force, a gradient in E^2 would be even steeper for A^2 due to the frequency shifting. Indeed, the steeper gradient induced by ionization of argon leads to a $-\partial E^2/\partial x$ that is almost twice that observed in the pre-ionized/helium case. As a consequence, the wakefield amplitude is observed to grow significantly faster in the simulation with argon ionization, leading to an increased degree of pulse compression.

4. Conclusion

In conclusion, we report on an effective enhancement of self-compression of laser pulses in a plasma wakefield by using the frequency shifts induced by the ionization gradient in higher-Z gas relative to helium. Ionization-induced pulse steepening leads to a greater ponderomotive force that subsequently enhances the wakefield generation and therefore pulse compression. It may be difficult to use this wakefield enhancement process for electron acceleration since long propagation distances would be required that may be susceptible to filamentation instability. However, this could be used as a separate stage to seed a stronger gradient for wakefield generation in a subsequent pre-ionized plasma. As has been previously investigated, the laser contrast ratio can affect the electron acceleration [23], which may be due to ionization effects. Our study may shed light on future experiments where the ionization processes play a role. For example, laser beam imperfections in realistic experiments, such as hot spots, may lead to ionization filamentation. For pulse compression, optimal conditions can be found for a large range of pulse energies with appropriate choice of f-number for focusing and gas species, such that the pulse intensity is matched with the ionization intensity.

Acknowledgments

This work was funded by the NSF under grants No 0903557 and 1054164, and DARPA under contract N66001-11-1-4208. The authors acknowledge the OSIRIS Consortium, consisting of UCLA and IST (Lisbon, Portugal), for the use of the OSIRIS 2.0 framework.

References

[1] Schmid K *et al* 2009 *Phys. Rev. Lett.* **102** 12480
[2] Krausz F and Ivanov M 2009 *Rev. Mod. Phys.* **81** 163–234
[3] Couairon A and Mysyrowicz A 2007 *Phys. Rep.* **441** 47–189 ISSN 0370-1573
[4] Wagner N L, Gibson E A, Popmintchev T, Christov I P, Murnane M M and Kapteyn H C 2004 *Phys. Rev. Lett.* **93** 173902
[5] Chvykov V, Radier C, Cheriaux G, Kalinchenko G, Yanovsky V and Mourou G May Compression of ultra-high power laser pulses *Lasers and Electro-Optics (CLEO) and Quantum Electronics and Laser Science Conf. (QELS), 2010 (San Jose, CA)* pp 1–2
[6] Skobelev S A, Kim A V and Willi O 2012 *Phys. Rev. Lett.* **108** 123904
[7] Tsung F S, Ren C, Silva L O, Mori W B and Katsouleas T 2002 *Proc. Natl Acad. Sci.* **99** 29–32
[8] Ren C, Duda B J, Hemker R G, Mori W B, Katsouleas T, Antonsen T M and Mora P 2001 *Phys. Rev.* E **63** 026411
[9] Shorokhov O, Pukhov A and Kostyukov I 2003 *Phys. Rev. Lett.* **91** 265002
[10] Gordon D F, Hafizi B, Hubbard R F, Peñano J R, Sprangle P and Ting A 2003 *Phys. Rev. Lett.* **90** 215001
[11] Faure J, Glinec Y, Santos J J, Ewald F, Rousseau J P, Kiselev S, Pukhov A, Hosokai T and Malka V 2005 *Phys. Rev. Lett.* **95** 205003
[12] Schreiber J, Bellei C, Mangles S P D, Kamperidis C, Kneip S, Nagel S R, Palmer C A J, Rajeev P P, Streeter M J V and Najmudin Z 2010 *Phys. Rev. Lett.* **105** 235003

[13] Balakin A A, Litvak A G, Mironov V A and Skobelev S A 2012 *Europhys. Lett.* **100** 34002

[14] Pipahl A, Anashkina E A, Toncian M, Toncian T, Skobelev S A, Bashinov A V, Gonoskov A A, Willi O and Kim A V 2013 *Phys. Rev.* E **87** 033104

[15] Kim A V, Lirin S F, Sergeev A M, Vanin E V and Stenflo L 1990 *Phys. Rev.* A **42** 2493–5

[16] Fonseca R *et al* 2002 Osiris: A three-dimensional, fully relativistic particle in cell code for modeling plasma based accelerators *Computational Science—ICCS 2002* (*Lecture Notes in Computer Science* vol 2331) ed P Sloot *et al* (Berlin: Springer) pp 342–51

[17] Sprangle P, Esarey E and Hafizi B 1997 *Phys. Rev. Lett.* **79** 1046–9

[18] Ammosov M V, Delone N B and Krainov V P 1986 *Sov. Phys.—JETP* **64** 1191–4

[19] Wigner E 1932 *Phys. Rev.* **40** 749–59

[20] Wood W M, Siders C W and Downer M C 1991 *Phys. Rev. Lett.* **67** 3523–6

[21] Esarey E, Ting A and Sprangle P 1990 *Phys. Rev.* A **42** 3526–31

[22] Quesnel B and Mora P 1998 *Phys. Rev.* E **58** 3719–32

[23] Mangles S P D *et al* 2006 *Plasma Phys. Control. Fusion* **48** B83